IEEE Access
Multidisciplinary | Rapid Review | Open Access Journal

Received 29 March 2023, accepted 10 April 2023, date of publication 19 April 2023, date of current version 24 April 2023.

Digital Object Identifier 10.1109/ACCESS.2023.3268536

RESEARCH ARTICLE

Innovative Technology for Production of Electrical Cabinets Using Laminated Conductors

MARIJA ODAK[1], JOSIPA STEGIĆ[1], IGOR ERCEG[1], (Member, IEEE), DAMIR SUMINA[1], AND ELVEDIN TOPČAGIĆ[2]

[1]Faculty of Electrical Engineering and Computing, University of Zagreb, 10000 Zagreb, Croatia
[2]Duplico Ltd., 10431 Sveta Nedelja, Croatia

Corresponding author: Marija Odak (marija.odak@fer.hr)

This work was supported by the European Regional Development Fund through the project "Development of technology for connecting components of control electrical cabinets using laminated conductors" under Grant KK.01.2.1.02.0003.

ABSTRACT Electrical cabinets are assembled manually to a great extent. The existing wiring technology of electrical cabinets is a big consumer of plastic materials used for the wire ducts which make up a large portion of the cabinet volume. Also, the current electrical cabinet production requires a lot of human labor. This paper proposes a new laminated conductor technology used for connecting electrical cabinet components. The approach is based on alternately stacking conductive and insulating layers. The primary advantage of the new technology is the possibility of accomplishing a fully automated production by using laminated conductors of rectangular cross sections for interconnecting the components. Additional benefits are reduced size, approximately by 70%; and a simplified use and installation. Both thermal and mechanical simulation analyses were carried out in the study. The final product of this technological development and its application is a prototype, which was evaluated experimentally for its electrical and mechanical functionality. Thermal conditions were also tested. The tests that were performed in this study include also mechanical testing on the bolts in the circuit block and electrical current tests. The experimental results justify the application of the proposed technology.

INDEX TERMS Automation, conductors, electrical equipment industry, production engineering, technological innovation.

I. INTRODUCTION

Electrical cabinets are widely used in industry, mostly as housings for various switching, control, and other devices that are generally utilized to monitor and control electrical and mechanical processes. Because more and more sectors use completely automated production, there is also an increase in demand for automated production of electrical cabinets. Wire ducts are used for housings the wires that connect the equipment inside an electrical cabinet [1]. That traditional method of wiring, which involves physical work, is a tiresome and time-consuming task that extends delivery times and increases the risk of error [2]. The size of the electrical cabinet is directly influenced by the number of wire ducts used for wiring, making it challenging to install. For example, installing control cabinets in a city train environment could be difficult due to the handling process, which can cause arm and waist fatigue in workers [3]. Additionally, due to the abundance of wire ducts, typical cabinets utilize a lot of plastic, and one of the key objectives of the European Union (EU) is to reduce plastic use [4].

This paper proposes a development of a cutting-edge technology to automate the production of control electrical cabinets, which consist of conductive and insulating layers placed alternately, followed by a final insulation plate with integrated electrical devices. Considering that the engineer typically spends around two hours preparing the arrangement of a control cabinet of average size [5], this technology will make assembly much faster and easier. Production time, size, and plastic usage will be decreased. The conductive layer is made

The associate editor coordinating the review of this manuscript and approving it for publication was Zhiwu Li.

up of laminated conductors with rectangular cross sections that are arranged in accordance with the required standard. Both the conductive and insulating layers will be formed using a computer numerical control (CNC) machine.

First, a 3D computer-aided design (CAD) model was created for a specific electrical cabinet with a defined equipment configuration. The volume of the cabinet was reduced by 70% by substituting the standard cabinet for a cabinet with laminated conductors (see Fig. 1). Using cost-utility optimization, the materials for the conductive and insulating layers were chosen in accordance with the properties given in [6], [7], [8]. The CAD model mentioned above was used in thermal and mechanical simulations, which were performed using the ''Siemens NX'' software [9] and its add-on called ''Simcenter FloEFD'' [10]. The results of the thermal simulations were achieved by determining the input and output current of the assembly together with the corresponding rated diversity factor (RDF). A finite element analysis was performed to analyze the model, with the mesh properties set according to [11]. When developing a thermal field model, heat transfer through both radiation and convection towards the environment were taken into consideration [12]. Multiple simulations were run for stationary state and time dependence. The obtained values were then utilized to optimize the placement of conductors, insulating plates, and ventilation apertures [13], [14].

After the simulations, heat conditions were tested experimentally. In addition, mechanical simulations of tensile forces and shear stress exerted on the bolt and of the force needed to tighten the bolt until the thread breaks were performed. The findings of these simulations are presented in this study. Some assumptions or model simplifications (no friction or sliding involved, bolts and washers without threads) were made to simulate the clamping processes, which could lead to outcomes that differ from the real scenario [15], [16], [17], [18].

The prototype was made after the final version of the CAD model was optimized. The conductors and insulation plates were cut to the required sizes and shapes using a CNC machine. They were then set out in accordance with the predetermined arrangement, and finally, conductive bolts were used to secure the electrical equipment on the final upper insulation plate. Since it is well known that the contact resistance is dependent on complex physical processes, many of which have a random nature, its analytical computation is subject to significant errors [19]. The presence of contact connections can increase resistance, as well as the heating of the electrical equipment. As a result, the outcomes of simulation and experimental testing may differ [20], [21], [22]. To reduce contact resistance, the total area of electrical connection must be as large as possible [23].

Once the assembly was complete, the experimental testing of the proposed innovative technology was carried out. First, a single layer of conductors and an insulating plate were tested in a lab environment for their thermal properties using a nominal current flow. The benefits and drawbacks of the present design were identified using temperature probes and a thermal camera [24]. Furthermore, electrical and mechanical tests were performed, including dielectric testing, peak current testing, and short circuit current testing, as well as tensile testing of the screw connection, tensile testing of the bolts, flexural testing of the bolts and the testing of the bolts in the switch block by tightening them with a torque wrench. All the tests were conducted in accordance with the relevant standards of the International Electrotechnical Commission (IEC) 61439-1 and IEC 61439-2 [25], [26]. The application of the new technology was successfully confirmed.

The paper is organized as follows. Section II provides insight into the technology concept and development of a 3D model in accordance with the required standards. Section III presents the thermal simulation parameters, settings and the obtained results. Section IV gives an overview of mechanical simulations, their parameters and the obtained results, including shear stress and tensile stress simulations. The findings of the experimental verification of the new technology concept are reported in section V. Finally, in the conclusion, the results of the study are summarized and future activities outlined.

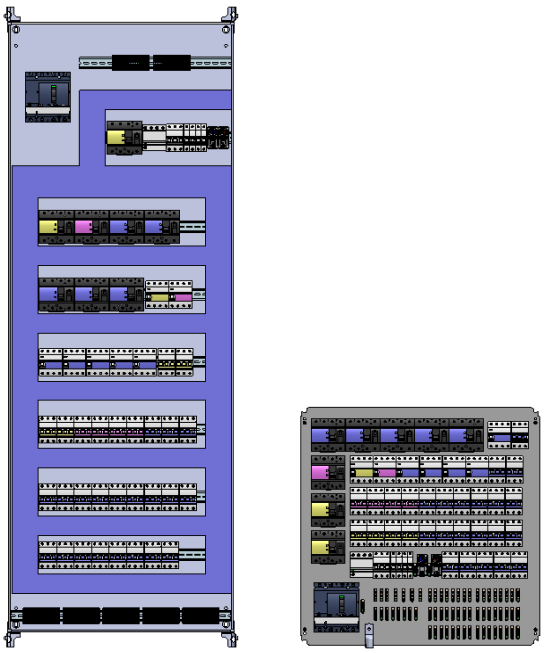

(a) Existing technology (b) Proposed technology

FIGURE 1. CAD model of mounting plates incorporating the same equipment.

II. TECHNOLOGY CONCEPT

The first step in the technology development was adapting to relevant standards and design specifications from [25] and [26]. It was necessary to define a method of interconnecting conductors on different layers of the assemblies and the equipment on the last layer. One of the challenges was fixing the equipment on the last layer. In the end, insulating plates and conductor materials were chosen, and the construction of a prototype began.

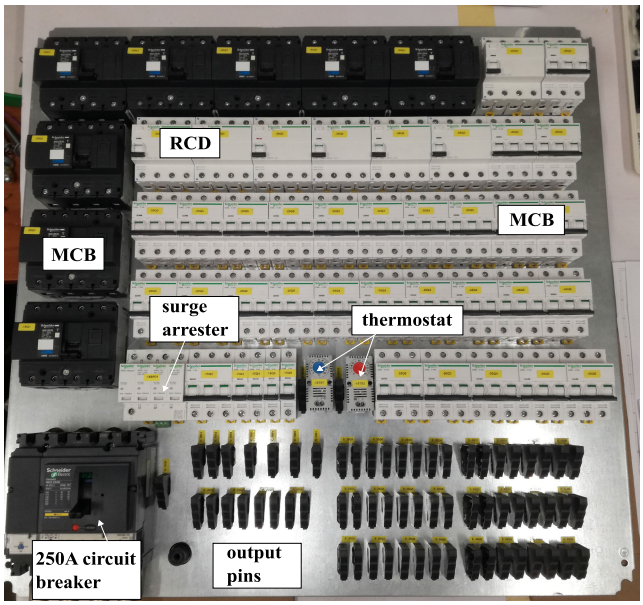

FIGURE 2. 800mm x 800mm mounting plate with electrical equipment.

A. DESIGN REQUIREMENTS

The type of a cabinet housing was determined after the equipment configuration had been decided upon. The cabinet based on the conventional technology used for laying the equipment has nominal housing dimensions of 2000 mm x 800 mm x 400 mm in height, width, and depth. A mounting plate with the measurements of 1897 mm x 696 mm x 27 mm is incorporated in the cabinet. The equipment was then mounted in the cabinet based on the technology proposed in the next stage. The nominal size of the cabinet based on the proposed technology is 800 mm x 800 mm x 300 mm, and a 750 mm x 750 mm x 2.5 mm mounting plate is used to hold the equipment in place. Fig. 2 provides a detailed overview of the equipment arrangement on the mounting plate. When comparing these two electrical cabinets, we can see that the volume for the same quantity of equipment is reduced up to 70% in the proposed cabinet design.

The final configuration of the equipment housed in the proposed electrical cabinet is a result of multiple iterations, in which the goal was to foresee potential issues, particularly regarding the arrangement of the conductive layers and the conductors that will interconnect this equipment. A short circuit between the mounting plate and the connecting elements of the conductive layers makes it impossible to place the equipment (electrical components connected to the laminated structures) on the mounting plate. Because of that, the mounting plate will make the first layer of the laminated structures on which the remaining layers will be piled, and the equipment placed on the insulating layer will have perforated channels leading to the laminated structures. Additionally, they have passages that match the mounting plate holes required to mount or fix the mounting plate to the cabinet structure.

B. CONNECTING PIN

The link that conveys the electric potential between the conductive layers of the laminated structures and the equipment was the next issue to be addressed while developing this innovative technology. As part of the study, various connection models were created utilizing conventional techniques for joining structural parts in the connector in the laminated structures. Due to the geometry of the equipment, e.g. fuses, feeders, and switches, it was decided to attach the equipment to the pin via a screw connection, i.e. a bolt. The concept of attaching pins and equipment on the laminated structures evolved into the first model. At this point, the development continued into two directions: one focused on creating pins to connect the conductive layers of the laminated structures, and the other focused on creating equipment that could connect to those pins. The interconnecting elements for joining the conductive layers within the laminated structures were incorporated over time and are now a part of the pin that joins the laminated structures to the electrical components of the assembly.

Since the models that were created had to take into account the needs of automated production in the future, the pin models based on welding were the first to be investigated. Because of lines with larger cross sections, where it would be difficult to connect the pin and the conductor and put them inside the laminated structures, this method is not viable. The following connection concept used a click pin with a mechanically secured pin to prevent unscrewing, as seen in Fig. 3. The points of contact (horizontal surfaces) between the lower conductive layer and the fixing element as well as between the fixing element and the top surface of the pin serve as the contact surfaces for transmitting electric potential under the pin. The issue with this design is the strengthening element, whose processing would be time-consuming and costly. Due to the aforementioned reasons, the usage of a pin that is fastened by a screw connection within the laminated structures has evolved into the standard technique of connection.

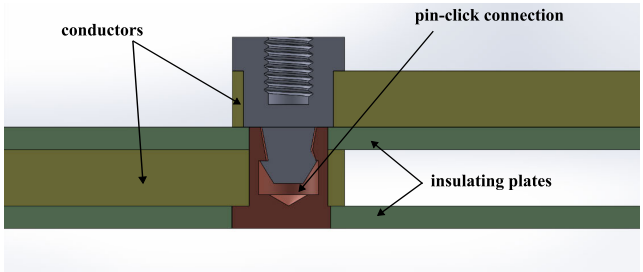

FIGURE 3. Laminated structure for pin-click connection.

C. LAMINATED STRUCTURE

The performance of joining and connecting the laminated structures correlates with the choice of the shape of the conductive layer. Compared to cutting the conductive layer and metal plate pieces, using conductors of circular cross sections e.g. a wire, results in less waste. Consequently, conductors

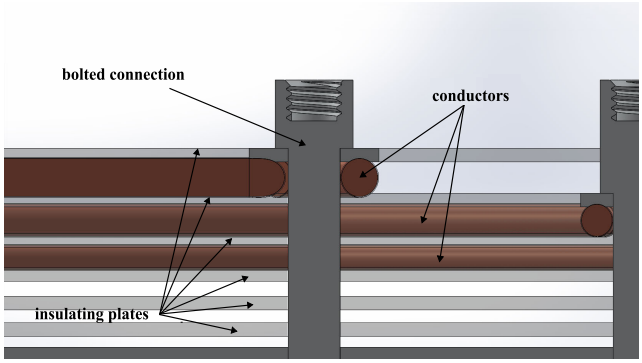

FIGURE 4. Connection made by means of conductor of circular cross section and a bolt.

of circular cross sections were the primary choice when it comes to the shape of conductors. In order to guarantee the shape of conductors along the conductive layer, they are to be placed in troughs created inside the insulating plates of the laminated structures. The pin is fastened with a nut on the output side after passing through the laminated structures. As a part of this concept, it is also proposed to use metal with milled troughs that would contain insulated conductors in place of insulator plates, as shown in Fig. 4. The possibility of welding the conductors to the supporting components of the screw connection inside the laminated structures was also studied as a concept, as seen in Fig. 5.

A screw connection consists of supporting elements for the electrical contact, a nut that, due to its geometry and shape, prevents the screw part of the laminated structures from being unscrewed, and either a pin for connecting the equipment or bolts for connecting conductive layers within the laminated structures. Between the conductive layers we want to connect, adjacent parts are placed in sequence. Drawbacks of this and the previous idea is the enormous bending radius of conductors with large cross sections, which would take up a lot of the space of the conductive layer, as well as the impossibility of using conductors with various cross sections in the same conductive layer.

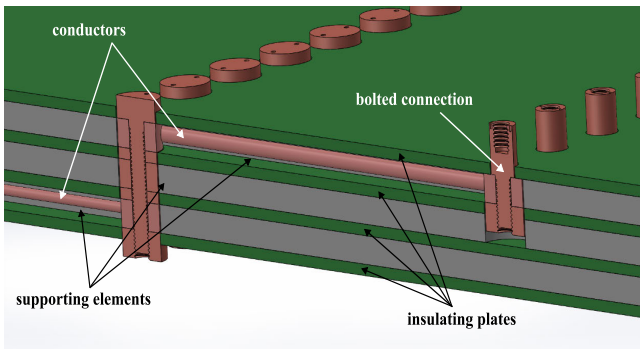

FIGURE 5. Connection using a conductor of circular cross section welded to supporting element.

Cutting the conductive layer of the laminated structures from an Al/Cu plate is an option that enables the possibility to arrange conductors of different cross sections, however of the same height, within the conductive layer. Additionally,

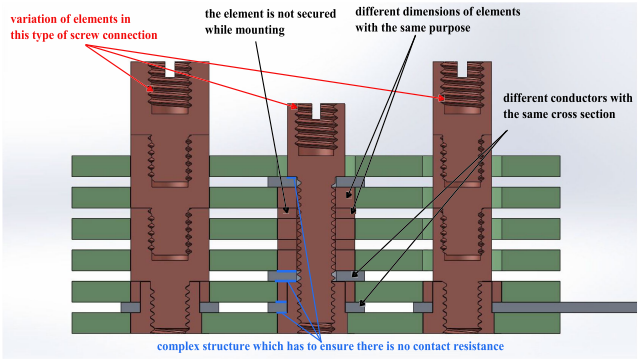

FIGURE 6. Connecting conductive layers using washers.

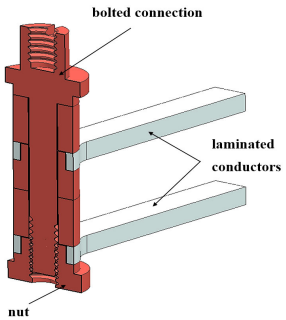

FIGURE 7. Joining laminated structures by means of a screw connection.

the overall laminated structure is more compact and stiff, the contact surface is flat, making it easier to achieve electrical contact. It is also feasible to unify the values, or the geometry of the elements. The model with solely screwed elements had a problem since it had elements with varied sizes serving the same function and there were circumstances in which contact between the conductor and the screwed element would not occur, as seen in Fig. 6. This led to the development of a new model that had a screw connection that connected the conductive layer using supporting components. By virtue of the design of the pin, laminated structures are also guaranteed, as is the generation of a pressure force within the screw connection. This type of joint is shown in Fig. 7, and in Fig. 8 an example of connecting a miniature circuit breaker (MCB) with conductive layers can be seen.

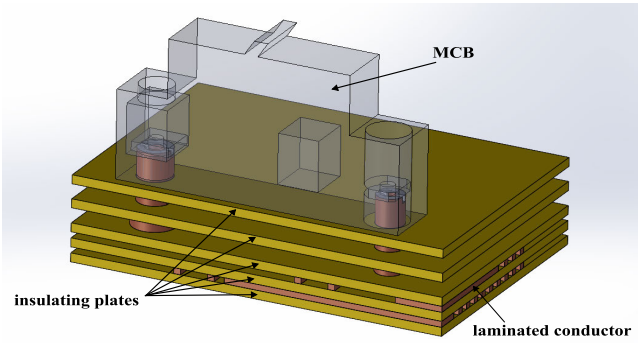

FIGURE 8. CAD model for connecting MCB to conductive layers.

The conductive layers are joined by supporting parts so that they can fit in between one another, and the clamping connection ensures that the electric potential is transmitted

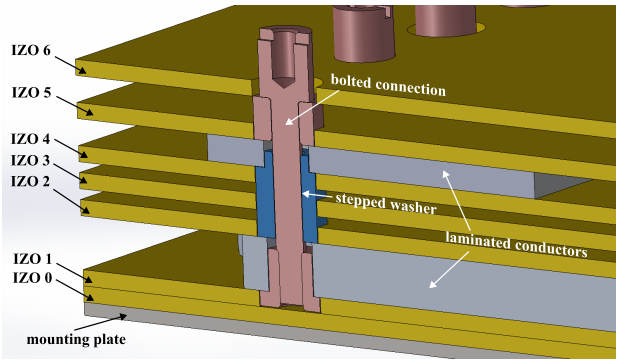

FIGURE 9. CAD model of joining laminated structures using a stepped washer.

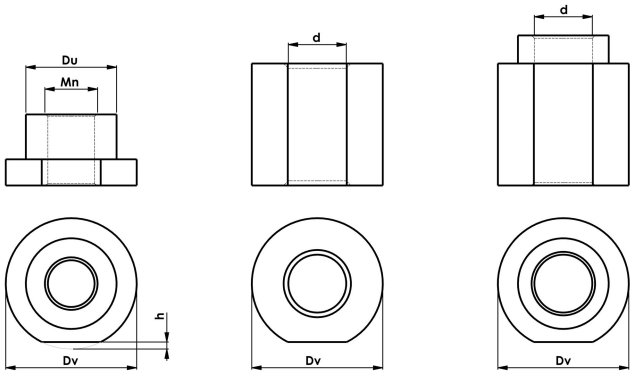

FIGURE 10. An illustration of clamping joint's nuts and washers in layered structures.

over the contact surfaces. There are two types of supporting elements: those that are attached to the conductive layer and those for transmitting the electric potential via the conductive layer. The model and element geometry must be made as simple as possible so as to create laminated structures, which was also achieved by combining the underlying elements, if there were several in a row, into one element. Additionally, the pin geometry was altered so that it uses less material and is no longer dependent on the insulating plate.

TABLE 1. Dimensions of nuts and washers for each cross section.

S (mm²)	Dv (mm)	Du (mm)	d (mm)	Mn (mm)	h (mm)
10	8	5.8	4.1	4	0.3
16	10	7.8	6.1	6	0.4
25	11	8.8	6.1	6	0.4
35	12	8.8	6.1	6	0.45
50	13	9.8	6.1	6	0.5
70	14	9.8	6.1	6	0.75
185	21	13.8	8.1	8	1.1

On the laminated structures, the electrical connection that serves also as a means of securing the equipment (such as electrical components) is made via a screw connection. The primary purpose of the nut is to produce a clamping connection. The nut is held in place in the related insulating layer by the geometry of the outer edge part with the cutout, which also prevents the nut from slipping when it is tightened. Accordingly, the corresponding locations in the insulating layers must match the geometry of the nut in that position enlarged by the necessary clearance for a simpler positioning during assembly. The clearances must be kept to a minimum so as not to damage the anti-slip protection of the nut. The nut, the washer (a type of washer used for transmitting electric potential), and the stepped washer presented in Fig. 9 (a designation for a second type of washer which connects the potentials between individual conductive layers) are geometrically defined by the current they conduct. Fig. 10 shows the nuts and washers of the clamping joint in the layered structure, and their dimensions are listed in Table 1. The cross section of a nut is denoted by S, the outer diameter of the nut or washer by Dv and the inner diameter of a nut by Du. The inner diameter of the washer is denoted by d, while Mn is the outer diameter of the nut thread. The nut and the washer have been cut out laterally for this type of connection, and h determines the depth of this cut-out.

The bolt used to secure the entire connection follows the geometry of the washers and has a unique value for the length of the bolt waist. That value depends on the conductive layer in which the clamp connection is made and the height of the equipment above the last insulating plate. That height must have a value large enough to make contact with the conductive part of the equipment which is on, i.e. above the insulating plate, because there must be a gap of up to 1 mm to prevent the equipment from resting on the back insulating plate. Otherwise, there is a counter force to the pressure force in the clamping joint.

D. SWITCHGEAR AND TERMINAL BLOCK DESIGN

The elements that interconnect the conductive layers and electrical equipment pass through the layered structure, and their paths are located corresponding to the position of the input on the equipment, in that way the bolted connection will fix the position of that element on the plate. For this reason, in the CAD model, the parts that are not capable of being connected from the bottom side are modeled to match the desired connection, or the cross section that connects to it. This adjustment can be seen in Fig. 11 and Fig. 12.

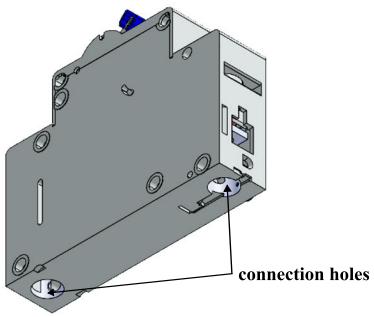

FIGURE 11. CAD model of MCB with additional passages for connection with laminated structure.

Fig. 13 displays a design proposed for connecting the terminal block. The model operates by using the spring principles, i.e. leaf and compression spring. The idea was that the mechanism would be inserted or clamped in the prototype,

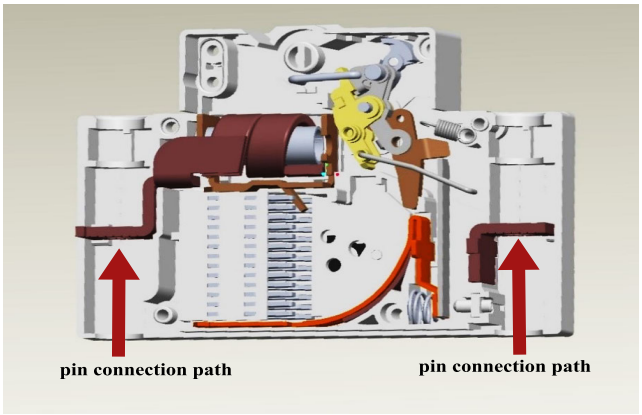

FIGURE 12. Cross section of a modified fuse.

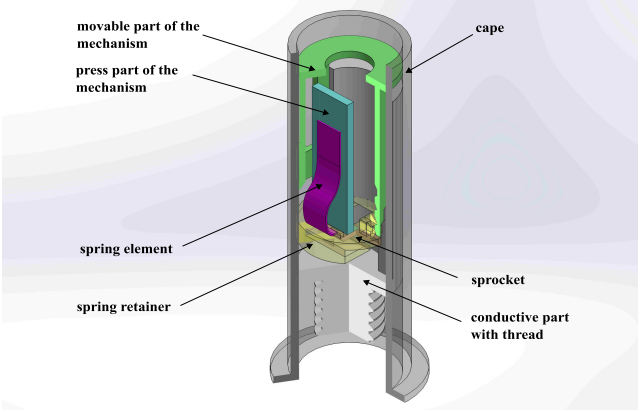

FIGURE 13. CAD model of plug-in mechanism for connecting terminal block.

with the outputs of standard clamps being positioned in the initial conductive layers of the prototype. The end of the conductor would be placed into this mechanism after stacking the laminated structures to the point where the conductor would made contact with the laminated structures. Because there must be space inside the laminated structures for their assembly, these ideas rely on the total height of the structures. The issue is that each plug-in element would be created for a certain cross section of the conductor, which would limit the functioning of the row clamp. For this reason, the already established screw connection principle must be used to construct the row clamp shown in Fig. 14.

E. INSULATING MATERIAL

For the selection of the insulating material a number of factors were taken into account, including adequate mechanical strength, electrical insulator properties, and market availability of plates with the required minimum size of 750 mm x 750 mm in width and height. For the initial prototype, pertinax 2061 with a 3 mm thickness was selected. To separate the components to be used for the connection to the conductive layers of the laminated structures, namely the nuts, which are located in the first insulation layer (IZO 1), the initial insulation board IZO 0 was placed on the mounting plate. Nuts are elements that are designed to achieve the clamping

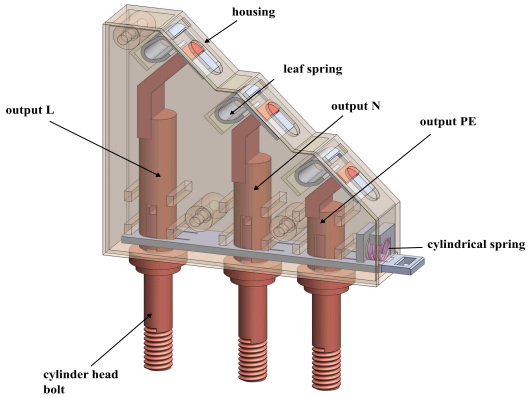

FIGURE 14. Series clamp model of laminated structures.

connection, i.e.,the contact between the location of the conductive layer, which corresponds to one of the positions of the joint on the element, and the conductive waist that leads the electric potential to the next contact location. The contact can be in another conductive layer, or directly on the element on the back mounting plate.

TABLE 2. Current resistance of insulated lines and cables that are not laid in the ground.

Cross section of a conductor (mm ^{2})	Copper conductor		Aluminum conductor	
	Current (A)	Fuse (A)	Current (A)	Fuse (A)
0.75	12	6		
1	15	10		
1.5	18	10		
2.5	26	20	20	16
4	34	25	27	20
6	44	35	35	25
10	61	50	48	35
16	82	63	64	50
25	108	80	85	63
35	135	100	105	80
50	168	125	132	100
70	207	160	163	125
95	250	200	197	160
120	292	250	230	200
150	335	250	263	200
185	382	315	301	250
240	453	400	357	315
300	504	400	409	315

F. CONDUCTOR MATERIAL

Copper conductor cross sections for specific currents are defined by IEC 61439-1 [25] and IEC 61439-2 [26]. The value of the cross section compared to copper for the same value of current is taken as a degree when aluminum is used to create the conductor. Dimensioning of conductive parts is done according to fuse currents for line protection, and the values are lower than the permitted current for the conductor whose cross section is intended for connection.

Copper and aluminum conductor cross sections in relation to current and fuse are shown in Table 2. Since aluminum will be used to make the conductors of the conductive layers, the cross sections used are a degree larger compared to the copper

conductor. The connecting elements of the laminated structures with sections from 1.5 mm^2 to 10 mm^2 were grouped into one group of 10 mm^2. The reason is the geometry of the connecting elements, i.e. the contact surface for very small sections; for 1.5 mm^2, the inner diameter of the washer is d = 4 mm, while the outer diameter should be D = 4.5 mm, if we take into account the bevels, which is not acceptable due to the calculation of strength of the clamp elements of up to 10 mm^2. The connecting elements of 10 mm^2 are designed as a clamping connection with an M4 bolt, and of 185 mm^2 as a clamping connection with an M8 bolt, while the rest (16 mm^2, 25 mm^2, 35 mm^2, and 50 mm^2) are designed with an M6 bolt. The connecting elements for the laminated structures will be made of copper due to better mechanical properties (copper is naturally harder, stronger and more ductile than aluminum), with a section of the conductive part corresponding to the currents of the aluminum conductor. This is done because the reference surface is the contact surface between the clamp washer and the conductor of the conductive joint, and since the conductor is aluminum, the contact surface must be adapted to it. The geometry of the washers, nuts and bolts is made according to the contact surface of the reference joint. For the sake of contact resistance in the aluminum-copper connection, the copper elements of the clamping connection must be nickel-plated and tin-plated.

G. LAYERING THE MODEL

The fixed positions of the elements on the final insulating layer serve as points between which the conductor is routed within the conductive layers of the laminated structures. The idea that the electrical current conductors that are supplying other parts should be placed first was a guiding principle in creating the model prototype. The first conductive layer (CL 1) is shown in Fig. 15. CL 2, i.e. a PE (protective earthing) conductor with a thickness of 5 mm, is placed in the same layer. The PE conductive layer is then covered with a new insulator, IZO 2, whose geometry matches that of conductive layer 1, meaning that it was trimmed not to cover this layer. On top of IZO 2, CL 3 is positioned. This layer directs the N conductor of the output from the feeders in the direction of the row clamps. The total height of CL 2, IZO 2 and CL 3 amounts 10 mm, which corresponds to the height of layer CL 1, that is, the insulation layer IZO 3 will cover both CL 1 and CL 3, because the upper surfaces of the mentioned layers are in the same plane. In the next two conductive layers of 2 mm, CL 4 and CL 5, the outputs of the MCBs are connected to the series clamps. Because of the decision to do this in these two conductive layers, the necessary space was gained for stretching the lines through the conductive layers, because otherwise they would have to bypass the entrances to the MCBs. That would be a reason for having an extra layer in the entire laminated structure, resulting in a higher cost in the material due to longer washers and bolts.

The conductors that connect every component of the final mounting plate, are interconnected in the conductive layers

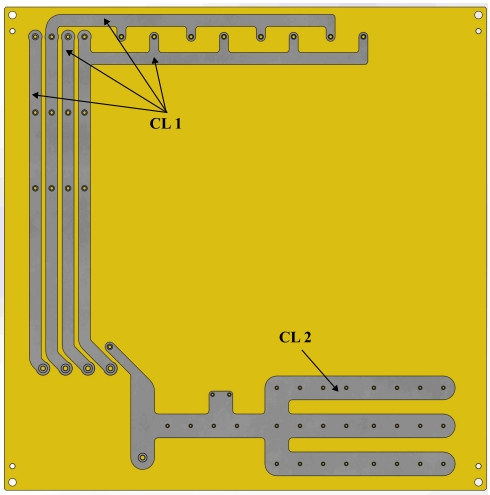

FIGURE 15. Stacking of CL 1 (L shape) and CL 2 (trident shape) on IZO 1; CAD model.

that come next. The separation is carried out through two conductive layers (CL 6 and CL 7) with a thickness of 5 mm due to the volume and geometry of the aluminum conductors. There is a place where the connection between conductive layers 6 and 7 is made only for that purpose using a separate screw; layer 6 can be seen in Fig.16. The screw head is positioned inside the insulating layer since the geometry is intended to stay inside the laminated structure.

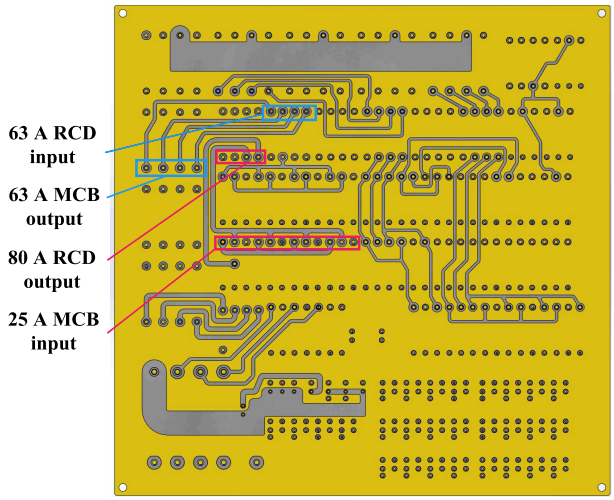

FIGURE 16. CAD model of CL 7 layered on IZO 6.

III. THERMAL SIMULATIONS

All the components of the assembly had to be simplified before running the simulations for a quicker and easier calculation. First, the heat source of the switchgear was established, and the geometry of the laminated conductors was determined. After that, the 3D model of the whole electrical cabinet underwent heat simulation. The prototype was constructed using the findings of this simulation as a guide.

A. DEFINING THE HEAT SOURCE IN THE SWITCHGEAR

Similar to a 3D model of a high power low voltage fuse from [27], the simulation of the 250 A circuit breaker was conducted using the ''Siemens NX'' add-on called ''Simcenter FloEFD''. The circuit breaker is defined as a heat source, considering that the switchgear will influence the heating of the entire assembly. Firstly, it was necessary to define the heat source in this electrical element. The possibilities for specifying the heat source inside the solid and hollow housing of the switchgear were analyzed. Heat losses amount approximately to 75 W, according to the statistics of 250 A circuit breakers [28]. In the first method, a heat source made up of three conductors with a combined radiation power of 75 W was distributed equally among the conductors inside the solid housing of the circuit breaker. Identical simulations were run for the hollow model of the switchgear. The housing of the modeled switch was made of Polytetrafluoroethylene (PTFE), and the conductors were made of copper.

The simulation results show that the use of current flow through the conductors was a more adequate choice for modeling heat losses in the circuit breaker. The total maximum temperature in the case of the solid switchgear was lower than in the case of the hollow switchgear, but the temperature on the sides of the element housing was lower in the case of the hollow switchgear. Table 3 shows a comparison of total maximum temperatures for both methods of the heat source determination discussed. From the results it can be seen that the most suitable method is precisely the one in which the currents (input/output) are defined on the conductors inside the circuit breaker. The other option for the heat source definition made the housing material melt, and it would also melt the insulating material used for insulating layers, because the maximum operating temperature of pertinax was 120 °C [29].

Table 3 shows that the temperatures on the housing of the circuit breaker were significantly lower than the total temperatures. A valuable preliminary conclusion is that the best choice for calculating the heating of switchgear is the method of defining current inputs and outputs. As expected, the temperature on the sides of the switchgear housing was lower in the case of the hollow housing.

B. SIMULATION OF ELECTRICAL CONDITIONS ON A 250A CIRCUIT BREAKER

To set up the simulation, calculation parameters were defined, such as type of analysis, physical features, project fluid and material. It was necessary to define the fluid subdomain in the circuit breaker enclosure with a wall thickness of 2 mm. The modeled circuit breaker is shown in Fig. 17. The copper conductors are modeled to rest against the aluminium pins entering the circuit breaker. The current through the aluminum pins comes inside the circuit breaker and flows through the copper conductors. The simulation was run for the total output currents that the RDF was applied to. The calculation yielded a maximum total temperature of 36.77 °C, which occurred on the copper conductor of the first phase.

TABLE 3. Maximum temperatures of circuit breaker.

	Max. temperature - total		Max. temperature - housing	
	Full	Hollow	Full	Hollow
Case 1	362.82 °C	346.48 °C	151.48 °C	91.14 °C
Case 2	28.84 °C	25.21 °C	36.96 °C	45.81 °C

C. CHOOSING THE SHAPE OF LAMINATED CONDUCTORS

Since the joints of the laminated conductors are expected to heat up the most, a lot of effort was put into determining the best way of finishing the laminated conductors. Two versions, out of the many that were fully studied, are presented and compared.

The simulation of current flow via conductors of various shapes assisted in the selection of a satisfying shape. Conductors with a curved edges were compared to those with a sharp edges both having the same cross section of 2.5 mm^2. By simulating current flow, results of Joule heating of the conductor were obtained. The current flowing through the conductors had a value of 10 A.

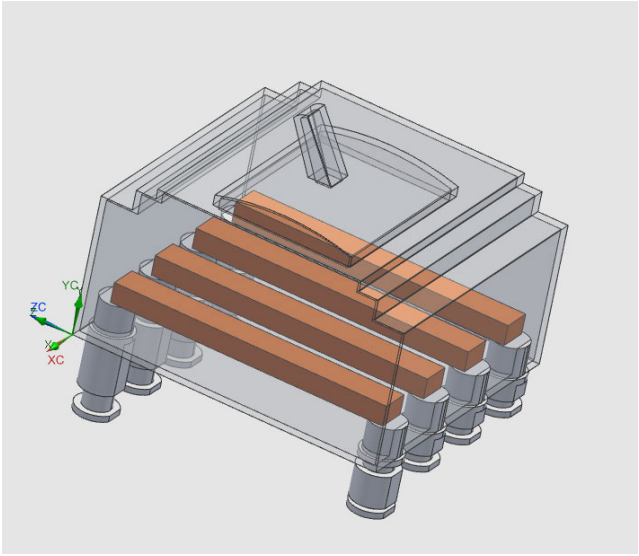

FIGURE 17. CAD model of a circuit breaker.

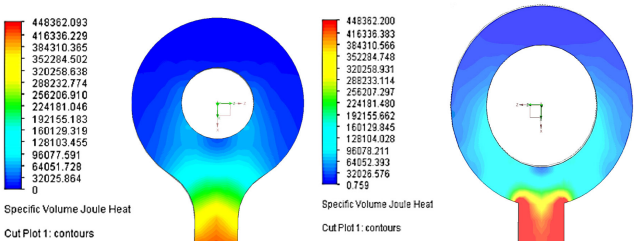

(a) Curved edges (b) Sharp edges

FIGURE 18. Distribution of heat on conductors, Specific Volume Joule Heat (W/m^3) scaled.

Firstly, a simulation with curved edges conductor was carried out. The maximum total temperature of the conductor was 28.98 °C. The next simulation was obtained on the

conductor with sharp edges. The maximum total temperature of the conductor was 29.02 °C. In the next figure (Fig. 18) the heating of two conductors of the same cross section, through which the same current (10 A) flows, but with different geometries, is shown. The results are displayed on an equal scale in [W/m^3] to identify the critical area where there is more heating. The conductor in Fig. 18b has higher temperatures due to its sharp edges, and the heating is concentrated at these ''edges''.

This investigation resulted in the selection of the conductor geometry. Since the sharp-edged conductor showed higher heating and higher current density near the edges, curve-edged conductors were chosen for the development of the prototype.

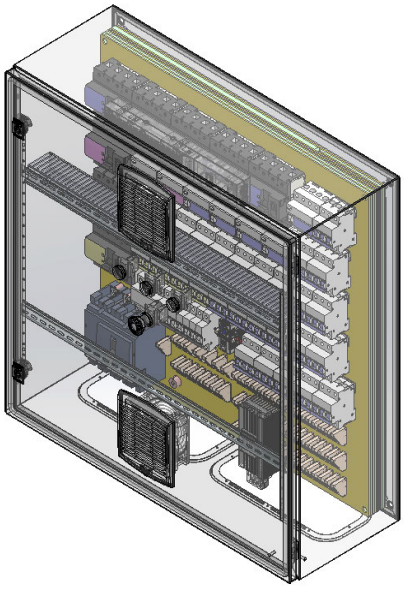

FIGURE 19. Isometric view of electrical cabinet with laminated structures and all equipment.

D. MODEL OF THERMAL SIMULATIONS

The subject of this investigation was a prototype of a low-voltage electrical cabinet for indoor use. Thermal simulations were carried out using the 3D CAD model displayed in Fig 19. The assembly was made up of a steel enclosure with air vents in the door, a mounting plate placed inside with a set of vertically placed insulating plates on the top, and laminated conductors passing through the plates. According to the requirements of the applicable standards [25] and [26], conductors of rectangular cross sections were positioned between the insulating plates. Interconnection is made by using conductive bolts through the layers.

A simpler design of the cabinet housing, switchgear, ventilation apertures, and screw connections was used to speed up and simplify the computation. The model used for calculations is shown in Fig. 20. The assembly was housed in a steel enclosure and had layers of conductors, insulators, and switching electronics. The model housing was 800 mm x 800 mm x 300 mm in size and had a 1.5 mm sheet thickness and two openings: a bottom air inlet and an upper air outlet. The openings measured 125 mm x 125 mm. To obtain the results of the overall heating, it was necessary to simulate currents flowing through the both conductors in the layers and the conductors in the switching devices.

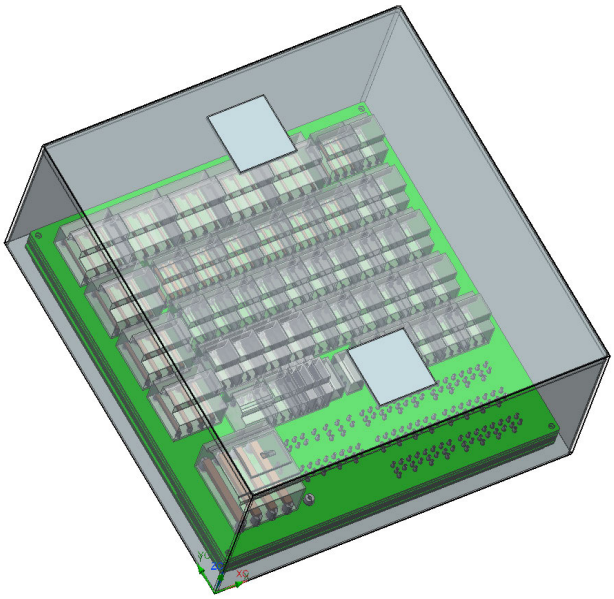

FIGURE 20. Simplified simulation model.

To examine the heat distribution in the cabinet and identify critical heat areas, a steady-state thermal simulation of the assembly was run. The simulation did not include any heat sources, but it did specify the electrical condition at the ends of the conductors. The Joule effect was caused by the current flow heating the conductors, which then heated also the rest of the assembly. An analysis of how electric current affects the heating of the electrical components, conductive materials, and insulating layers was provided by the simulation. To provide more realistic operating conditions, the existing values were modified using the RDF with a value of 0.6. Conduction, convection, and radiation are the three types of heat transfer that have an overall impact on temperature in these simulations. A computational fluid dynamics (CFD) add-on to the simulating software ''Siemens NX'' called ''Simcenter FloEFD'' was used to perform thermal simulations.

Firstly, it was necessary to set up calculation parameters. The type of analysis was set to internal, and the physical properties of radiation, gravity, and heat conduction in solids were checked. Gravity was adjusted on the y-axis as the observed control cabinet needed to be positioned vertically in space. Choosing the default solid, in this case aluminum, as well as the default fluid, i.e. air, was set in accordance with the specifications. The heat transmission coefficient, a value of 5.5 W/m^2/K, was the outer wall thermal condition default for wall conditions. The hollow switchgear and the casing of the control cabinet needed to be specified as fluid subdomains. Some of the material properties, such as those of aluminum, copper, or steel, were preset in the software, while others were defined by the user. Materials used for this electrical cabinet

include steel for the housing and mounting plate, pertinax for the insulating plates, and copper and aluminum for the conductive bolts and the laminated conductors. The input and output current defined on the conductors, conductive bolts and conductors inside the switchgear caused the assembly temperature to increase.

The mesh is a crucial part of the CFD study considering that the mesh parameter settings have an impact on the outcomes. The model was modified for this reason to eliminate the components that are irrelevant for the thermal analysis (knobs on the door, fillets on the screws, chamfers etc.). To shorten the calculation time, simpler models were used to substitute each complex part in the assembly. For each component of the assembly, mesh features were manually set at refinement levels from 1 to 9. More precise Joule heating results were achieved by setting the local mesh with a finer mesh resolution for each small conductive part independently. The cells were complex polyhedrons near the edges and rectangular parallelepipeds. The model contained 1,981,418 cells in total. In this instance, the internal analysis of the assembly was used, and the inlet and outlet of the ventilation apertures were specified. The housing of the electrical cabinet that was entirely closed with lids and acted as a fluid subdomain confined the internal airflow. The interior and exterior spaces of the enclosure as well as those of the electrical components were both filled with air that complied with standard atmospheric conditions. The basic simulation is run under standard atmospheric conditions with the ambient pressure of 101,325 Pa and temperatures of 20 °C and 40 °C. The lids on the ventilation openings were used to define the boundary conditions. The ambient pressure was set at the ventilation outlet lid and the inlet volume flow at the ventilation inlet lid had a value of 85 m ^{3}/h.

E. THERMAL SIMULATION RESULTS

To investigate the impact of the environment on the observed model, simulations were carried out in the same electrical conditions but at different ambient temperatures of 20 °C and 40 °C.

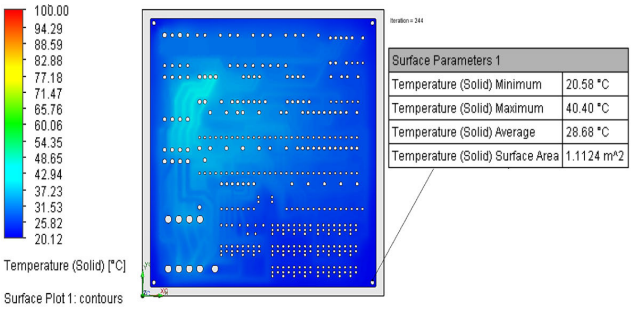

FIGURE 21. Distribution of heat across 5th insulating layer at 20 °C.

After the simulation was finished at 20 Â°C ambient temperature, the maximum temperature of the model in steady state was 40.45 °C. The conductor connecting the 80 A circuit breaker and the 80 A residual current device (RCD) generated the most heat. More attention needed to be paid

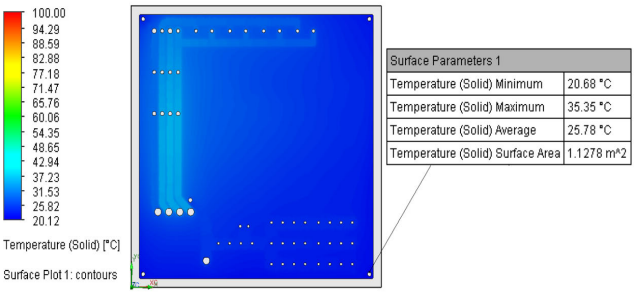

FIGURE 22. Distribution of heat across 1st insulating layer at 20 °C.

to the temperatures and heat distributions on the insulating layers, conductors, and screw joints. The conductors connecting the 80 A RCD to 25 A MCBs, as shown in Fig. 21, produced the most heat across the fifth insulating layer due to the Joule effect. Based on the obtained results, the maximum temperature of the final two layers, sixth and seventh, was the same as the maximum temperature of the entire assembly. Due to its exposure to the air, the average temperature of the top (seventh) insulating layer was lower than that of the sixth layer.

Due to the build-up of heat within the layered structure of the model, the average temperature of the fifth layer rose in comparison to the preceding layers. Since the maximum temperature typically decreases as the distance from the site of greatest heat accumulation increases, due to conduction, the average temperature of the following layers decreased. The phase conductors with the largest cross section were positioned on the first insulating layer. These conductors transmitted the highest value of current. The heat dispersion across the first layer is shown in Fig. 22. Table 4 displays the maximum, minimum, and average temperature values for various assembly layers.

TABLE 4. The assembly heat distribution at ambient temperature 20°C.

Assembly layer	Minimum temperature (°C)	Maximum temperature (°C)	Average temperature (°C)
mounting plate	21.49	31.73	25.37
IZO 1	20.68	35.35	25.78
IZO 2	20.62	33.91	26.38
IZO 3	20.58	35.52	28.01
IZO 4	20.57	37.35	28.56
IZO 5	20.58	40.40	28.67
IZO 6	20.54	40.45	27.99
IZO 7	20.12	40.45	26.97
enclosure	20.30	24.31	21.06

Thermal simulation results at the ambient temperature of 40 °C show that the maximum temperature of the model at stationary state amounts to 58.44 °C. It is an increase of 18.44 °C above the external ambient temperature. At an ambient temperature of 40 °C, the fifth layer of the model, where the conductors that heat up the most are located, has a temperature distribution as shown in Fig. 23. As expected, there is an increase in all temperature readings when compared to the model at an ambient temperature of 20 °C

(see Fig. 21). The distribution of heat across the first insulating layer is shown in Fig. 24. The minimum, maximum and average temperatures increased compared to the same layer in the previously performed simulation at an ambient temperature of 20 °C (see Fig. 22).

The temperature values for several assembly layers are shown in Table 5 including their minimum, maximum and average values. The temperature rise results obtained using the thermal simulation meet all criteria set forth in the applicable standard [25] and [26].

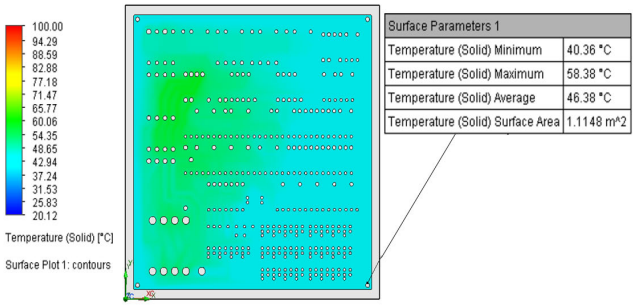

FIGURE 23. Distribution of heat across 5th insulating layer at 40 °C.

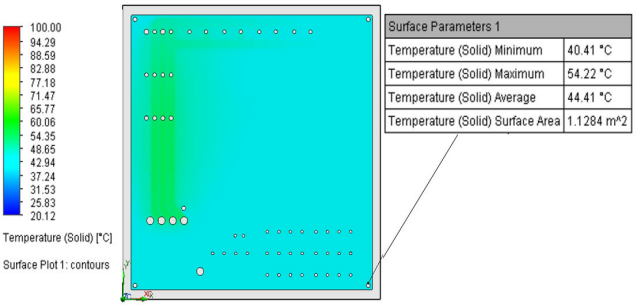

FIGURE 24. Distribution of heat across 1st insulating layer at 40 °C.

TABLE 5. The assembly heat distribution at ambient temperature 40°C.

Assembly layer	Minimum temperature (°C)	Maximum temperature (°C)	Average temperature (°C)
mounting plate	40.78	50.70	44.07
IZO 1	40.41	54.22	44.41
IZO 2	40.39	52.59	44.45
IZO 3	40.38	54.37	45.96
IZO 4	40.35	55.78	46.44
IZO 5	40.36	58.38	46.38
IZO 6	40.22	58.44	45.97
IZO 7	40.04	58.44	45.19
enclosure	40.16	43.97	40.79

F. TIME-DEPENDENT SIMULATION

In order to analyze the heat accumulation in the electrical cabinet, a time-dependent simulation was performed for the model at ambient temperatures of 20 °C and 40 °C. The simulation time frame was set to 72 hours. The simulation step was set to 60 seconds. According to the values the user entered, the simulation results were recorded. The final results are presented graphically in Fig. 25, and it can be noticed that the temperature rises gradually until it reaches a steady state value in 12 hours and then fluctuates around it. As expected, the rate of temperature rise in the first hour is higher in the simulation with an ambient temperature of 20 °C. As seen in Fig. 25, T_1 represents the temperature rise as a function of time for the model operating at an ambient temperature of 20 °C, and T_2 indicates the temperature of the model operating at an ambient temperature of 40 °C.

G. TEMPERATURE RISE VERIFICATION

The results must comply with the specifications of the relevant standard in order to be valid. As stated in subsection III-E, the highest total temperature recorded for a model at an ambient temperature of 20 °C is 40.45 °C, which is an increase of 20.45 °C above the ambient temperature. The highest total temperature of a model at an ambient temperature of 40 °C is 58.44 °C, which is an increase of 18.44 °C above the ambient temperature. As shown in Table 6, all the requirements of IEC 61439-1 [25] and IEC 61439-2 [26] standards have been fulfilled.

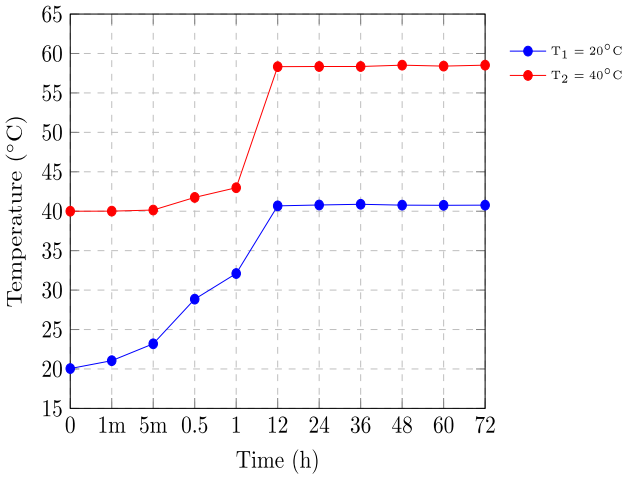

FIGURE 25. Temperature rise as a function of time.

TABLE 6. Temperature rise requirements.

Part of the assembly	Temperature rise condition	Temperature value at ambient temperature 20 °C	Temperature value at ambient temperature 40 °C
Manual operating means of metal	+15 °C	24.31 °C	43.97 °C
Manual operating means of insulating material	+25 °C	22.23 °C	41.72 °C
Accessible external metal surfaces	+30 °C	24.31 °C	43.97 °C
Accessible external insulating surfaces	+40 °C	24.31 °C	43.97 °C
Terminals for external insulated conductors	+70 °C	40.45 °C	58.32 °C

IV. MODEL FOR MECHANICAL SIMULATIONS

In order to compare the two types of joints and evaluate them in the assembly in terms of mechanical stress, mechanical simulations were carried out.

A. MECHANICAL SIMULATION MODEL

A piece that was extracted from the electrical cabinet assembly served as the basis for the CAD model on which mechanical simulations were run. The same materials were employed to compare the simulation findings for the two types of joints.

In the first scenario, the bolt exits the assembly through the final upper insulation layer. The modified switching devices are mounted on the bolt head, which is located outside the sandwich framework. A section of the conductor positioned in the final layer of the sandwich structure and an adjusted washer (see Fig. 26a) are both depicted on the model.

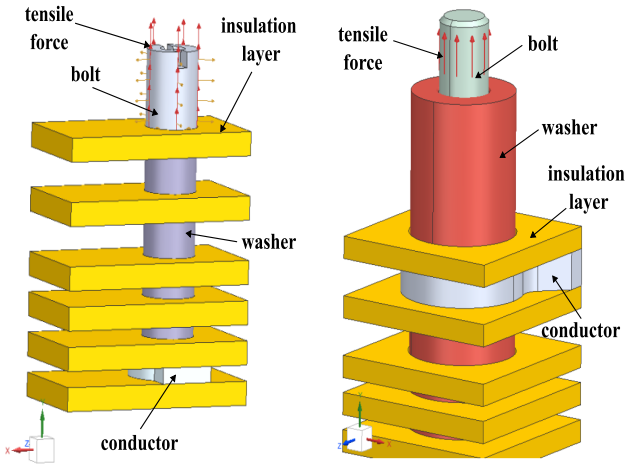

(a) First scenario (b) Second scenario

FIGURE 26. Position of tensile forces on the bolts.

Another situation is also simulated in which the bolt is inverted since it is possible to unscrew the bolt during regular operation. In other words, the bolt head is towards the cabinet rear. As a result, the mounting plate and the rear insulating layer would stop the bolt from being unscrewed.

In the second situation, the connection was made up of a bolt, two washers, and a copper conductor (see Fig. 26b). Properties of the materials used in the simulations of both scenarios are listed in Table 7. In this stage, different materials for insulation layers were still considered. In the simulations, FR4 was used, which had appropriate properties, as well as pertinax, which was used in other stages of the development. Constraints were set on the insulator plates that were fixed on all side surfaces. Other surfaces which were in contact with each other were defined with the function„Surface Gluing". The specified function linked the surfaces to prevent relative motion in all directions, allowing the load to be transferred from the bolt to other assembly components. The surfaces that were in contact with each other were defined manually. The analysis performed in NX was linear and the material was assumed to be permanently elastic and infinitely rigid. Hence, the results of the mechanical simulations show the elastic area and do not exceed the limit of elasticity, after which permanent elongation and fracture of the materials occurs.

TABLE 7. Properties of materials used in simulations.

	FR4 insulating material	Copper
Density (kg/mm^3)	$1.85 \cdot 10^{-6}$	$8.92 \cdot 10^{-6}$
Elastic limit (kPa)	$2178 \cdot 10^{5}$	3000
Young´s modulus (kPa)	13 000 000	114 000 000
Poisson´s coefficient	0.123	0.31

TABLE 8. Results of tensile stress simulation in the first scenario.

Tensile force (N)	Material displacement (mm)	Relative elongation (mm/mm)	Strain (MPa)
5	$7.89 \cdot 10^{-5}$	$1.54 \cdot 10^{-5}$	0.375
10	$1.58 \cdot 10^{-4}$	$2.34 \cdot 10^{-5}$	0.75
20	$3.16 \cdot 10^{-4}$	$4.69 \cdot 10^{-5}$	1.5
30	$4.73 \cdot 10^{-4}$	$7.03 \cdot 10^{-5}$	2.249
40	$6.31 \cdot 10^{-4}$	$9.38 \cdot 10^{-5}$	2.99
50	$7.89 \cdot 10^{-4}$	$1.17 \cdot 10^{-4}$	3.749

B. TENSILE STRESS SIMULATION

The simulation provides results for the tensile strength, which is a ratio of the maximum force F achieved during tensile testing to the initial cross section of the test sample A_0 and it is determined as follows:

$$\sigma = \frac{F}{A_0} \tag{1}$$

Different values of tensile forces were set, at which the mutual dependence of relative elongation and tensile stress was determined (see Tables 8 and 9). Graphical presentation of the results is shown only for the tensile force of 5 N). The total elongation was calculated for the assembly and on the cross section of the bolt. Relative elongation, ϵ was defined as the deformation or displacement of materials caused by stresses, expressed in (mm), and in this case it was calculated on the cross section of the assembly. The relative elongation was determined as follows:

$$\epsilon = \frac{\Delta L}{L_0} \tag{2}$$

where ΔL is the change in length after the test and L_0 is the initial value of the length. The tensile force was defined on the side surfaces of the bolt for both scenarios with the y-direction as shown in Fig. 26. The results are presented graphically in Section IV-D for a better analysis of the joint and with aim to detect critical points where the greatest stress would occur.

TABLE 9. Results of tensile stress simulation in the second scenario.

Tensile force (N)	Material displacement (mm)	Relative elongation (mm/mm)	Strain (MPa)
5	$8.67 \cdot 10^{-6}$	$7.4 \cdot 10^{-7}$	0.034
10	$1.73 \cdot 10^{-5}$	$1.48 \cdot 10^{-6}$	0.068
20	$3.47 \cdot 10^{-5}$	$2.9 \cdot 10^{-6}$	0.136
30	$5.3 \cdot 10^{-5}$	$4.45 \cdot 10^{-6}$	0.204
40	$6.94 \cdot 10^{-5}$	$5.93 \cdot 10^{-6}$	0.272
50	$8.67 \cdot 10^{-5}$	$7.4 \cdot 10^{-6}$	0.341

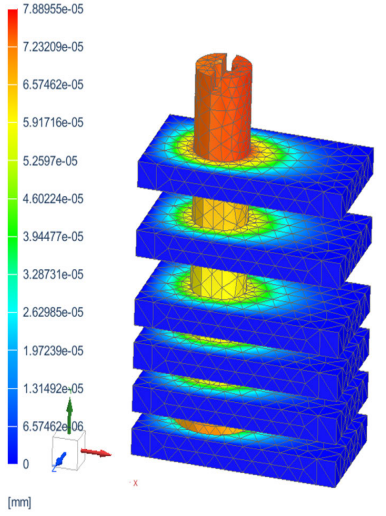

FIGURE 27. Total displacement in tensile stress simulation.

C. SHEAR STRESS SIMULATION

Shear stress is the ratio of the maximum force achieved during the shear test to the initial cross section of the test sample. The force was exerted on the side of the bolt body and acted in the direction of the x-axis to bend the bolt joint. Joint bending occurred in normal operation due to the gravitational force and the weight of the components that were placed on the output pins. Total elongations of the assembly caused by shear stress as well as total stresses and relative elongation on the cross section of the screw were obtained. Areas of the greatest stress can be identified on the graphic display of the data for the shear force of 5 N exerted on the complete assembly and the cross section of the assembly.

D. RESULTS OF TENSILE STRESS SIMULATION

In the first scenario, the results of the tensile stress simulation show that the maximum value of total displacement was reached at the screw head with a value of 0.0000789 mm when the tensile force was applied, as shown in Fig. 27. The maximum reached value of total elongation was 0.000154 mm and it was reached at the joints of the washers and insulating layers. The maximum stress in the first scenario was reached at the bolt head with a value of 0.375 MPa. The rest of the results for different tensile forces in the simulation of the first scenario are listed in Table 8.

In the second scenario, the maximum value of the total elongation for the tensile force with a value of 5 N exerted on the assembly amounted to 0.000008671 mm, located on the upper part of the bolt body. The maximum value of relative elongation was 0.000000741 mm/mm and was reached at the edges of the insulating layers as shown in Fig. 28. The highest stress was at the ''neck'' of the conductor, where it began to spread into,,the ring'', and the stress concentration was the highest. The proximity of the location where the conductor was fixed and the tensile force acted in the direction of the y-axis throughout the full surface of the bolt body contributed to this outcome. The maximum tensile strength in the second scenario was 0.341 MPa. The results for different tensile forces are listed in Table 9.

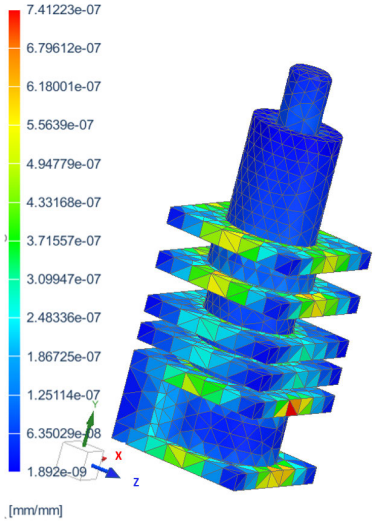

FIGURE 28. Relative tensile elongation of the assembly in the second scenario.

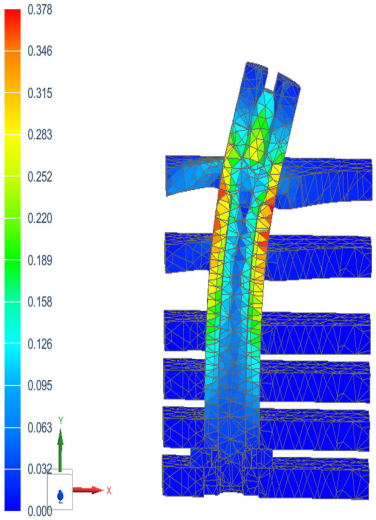

FIGURE 29. Maximum stress in shear stress simulation in the first scenario.

E. RESULTS OF SHEAR STRESS SIMULATION

In the first scenario, the maximum value of the total displacement for the applied shear force of 5 N was $5.1 \cdot 10^{-4}$ mm. The force was applied to the side of the bolt head. As expected, the largest material displacements were achieved at the top of the bolt head where the cross section was smaller. Fig. 29 shows the same result, but the deformations are shown as 10% of the model in initial conditions without the applied forces. The connection between the washer and the bolt on the first insulator plate was the place where the problem lay. The maximum stress was on the upper part of the washer with a value of 0.378 MPa. The maximum relative elongation was on the first insulating plate with a value of $3.368 \cdot 10^{-5}$ mm/mm.

In the second scenario the greatest elongation for the applied shear force of 5 N was 0.00007207 mm. It was achieved on the upper part of the bolt body like in the tensile stress case. In the second case, where the bolt was bent, the upper portion of the washer was under the most stress. The maximum value of the stress was 0.0914 MPa.

V. DISCUSSION ON ELECTROMAGNETIC COMPATIBILITY

The international standard IEC 61000 defines the general conditions and rules required for testing the electromagnetic compatibility (EMC) of almost all products with electronic or electrical circuits in order to ensure that they do not interfere with other electronic equipment or cause electromagnetic interference (EMI) that could impact the operation of nearby devices. The EU Directive [30] on EMC also defines the rules for placing electrical/electronic equipment on the market within the European Union.

Since the developed prototype does not contain any active electronic parts, it can be considered inherently benign. This means that the prototype cannot generate significant amounts of electromagnetic energy. Devices that are inherently benign in terms of electromagnetic compatibility are exempt from EMC testing [30]. Accordingly, it is not necessary to conduct the EMC testing for the developed prototype. However, the proper design and installation procedures [25] should be followed to reduce the possibility of EMI and guarantee an efficient operation of the electrical cabinet and any neighboring electronic equipment.

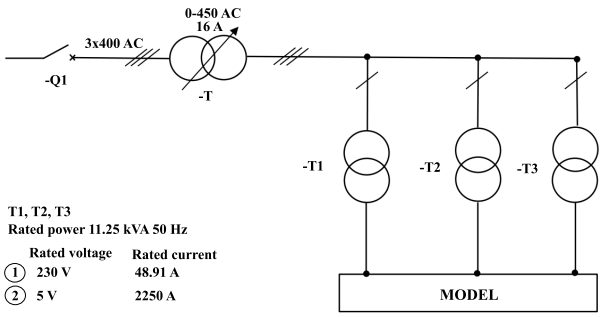

FIGURE 30. Schematic diagram of the heating test.

The future application of this technology includes connecting active components (e.g. soft starters, frequency converters, chargers for electric vehicles), so that full EMC testing for immunity and emission must be carried out for such prototypes.

VI. EXPERIMENTAL TESTING

In order to verify the technology according to the tests specified in the standards IEC 61439-1 [25] and IEC 61439-2 [26], a prototype was made that was identical to the 3D model used in the simulations. Heating testing including a current flow test, a dielectric test, a peak current value test and a short circuit current test was performed on the assembly or individual layers.

A. HEATING TESTS ON ONE LAYER

Transformers were used to finely regulate the conductor current during the experiments, as illustrated in Fig. 30. Using this combination, the current flowing across individual conductors can be controlled more precisely.

Temperature of the conductors was measured with a thermal camera FLIR T532 [24], and eight PT1000 temperature sensors glued to the conductors with a thermally conductive glue and connected to the data logger MultiCon [31] which was used to record temperatures (Fig. 31). This ensured that the findings of the temperature measurements taken by thermal camera could be traced and independently verified. Firstly, a 250 A current was set with the plate facing up, leaving the conductors uncovered and allowing radiation to further cool the system. This was not the case when the board and conductors are inside the sandwich structure during normal operation. That is why a different process was used, and the plate was turned towards the wooden surface in an effort to closely resemble the sandwich structure. With the plate turned, measurements were done using a current (with an RDF factor) of 220 A, measured in a stationary state, and an adjusted nominal current of 250 A, measured throughout the process at various moments during the stationary state. To ensure the readings were as accurate as possible, the thermal camera emissivity factor for the materials used in the assembly was established and a matting spray was applied to the conductors. In needs to be mentioned that the detected temperatures on the camera may have a measurement error, meaning that they display a temperature that is several degrees higher, due to reflections on the board and conductors.

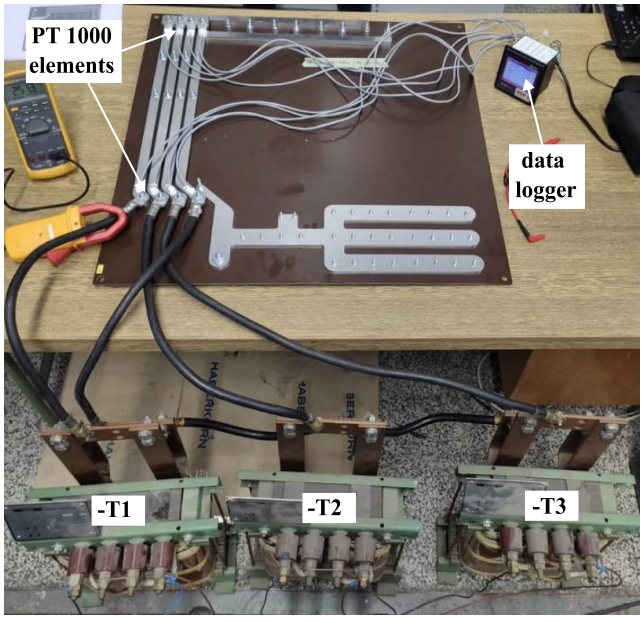

FIGURE 31. Configuration of the heating test.

The results of all heating tests indicate that the maximum temperature was reached in the second phase on the input connections. Because the L2 phase was heated by the adjacent

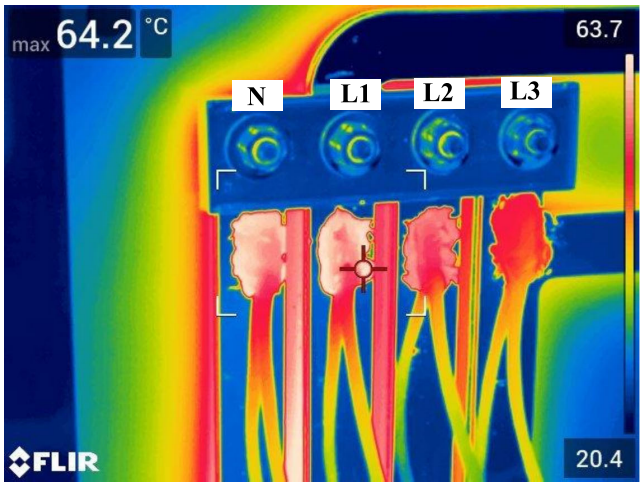

FIGURE 32. Display of temperature measurement on output contacts obtained with a thermal camera.

phases, the maximum temperature was also measured on the output contacts in the second phase (see Fig. 32). The least heating was on the PE conductor. In the first case, when the current was 250 A and the plate was facing up, the temperature at the input contacts in L2 was 78.9 °C and at the output contacts for the same phase it was 59 °C. After the plate was turned towards the wooden surface, temperatures were measured at the same locations in a steady state. The maximum temperature at the input contact was 91.7 °C and at the output it was 64 °C. In the last case, the current was set to 220 A and the temperature at the input contact of phase L2 was 71.6 °C, and at the output contact of the same phase was 53 °C. The observations revealed several discrepancies in the thermal calculations that were run. The temperatures were around 20 °C higher than in the simulation testing, and they were even higher on the supply side. The specified temperatures were the maximum temperatures that appeared on individual phases. These results led to the conclusion that the heating of the supply connection, which was not carried out as it would be on the prototype, was the cause of the heat build-up on the aluminum buses.

In laboratory conditions, the connection was made with M8 screws tightened with a torque of 20 Nm. For a smaller tightening torque, the contact resistance was higher and it resulted in even greater heating. Further tightening of the screw would cause the insulation board to fracture. The results of the tests conducted indicate that the next step should focus on measuring the heating of the contact joint, as it was done in the prototype. Additionally, it was necessary to create the contact joints outside of the prototype sandwich structure for a subsequent heating test. By doing this, it was ensured that a large amount of heat was kept outside the sandwich structure.

B. HEATING TEST OF THE PROTOTYPE

A prototype identical to the 3D model used for thermal simulations was made for an experimental heating test (see Fig. 33). Temperatures were measured in the LV switch block (without any other equipment) at different locations

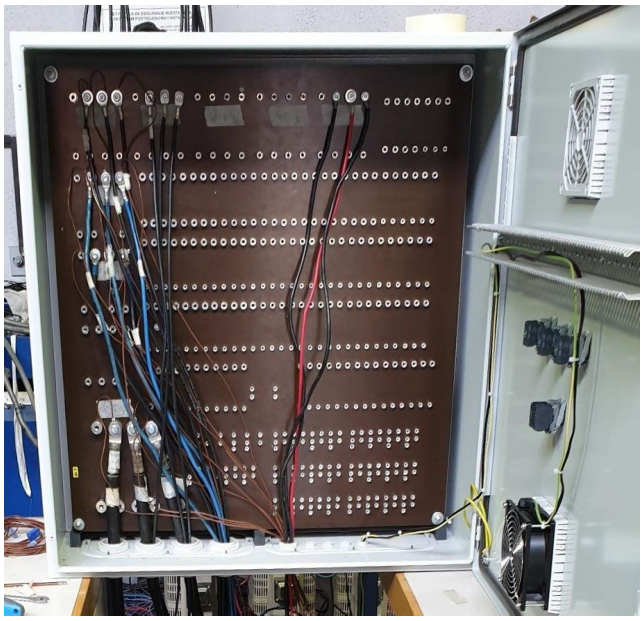

FIGURE 33. Prototype for experimental testings.

and after a steady state was reached in the heating test, the fan was turned on. The heating test was carried out with current of 250 A and a frequency of 50 Hz. Fig. 34 shows the measurement locations chosen for the heating test. The locations of the temperature probes are marked from 1 to 12. The two additional probes were located on the door and at the top of enclosure. The figure also shows values of the currents on individual inputs (250 A) and outputs (80 A, 63 A, 40 A).

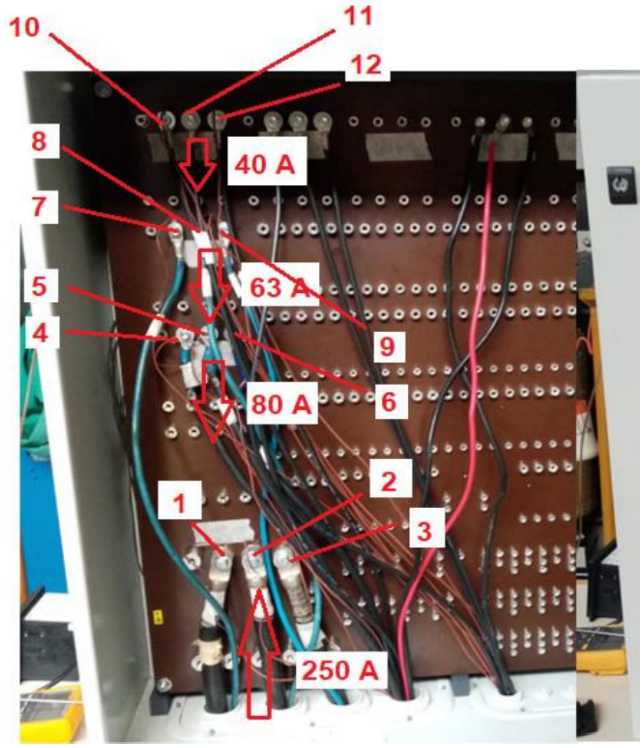

FIGURE 34. Locations of temperature probes.

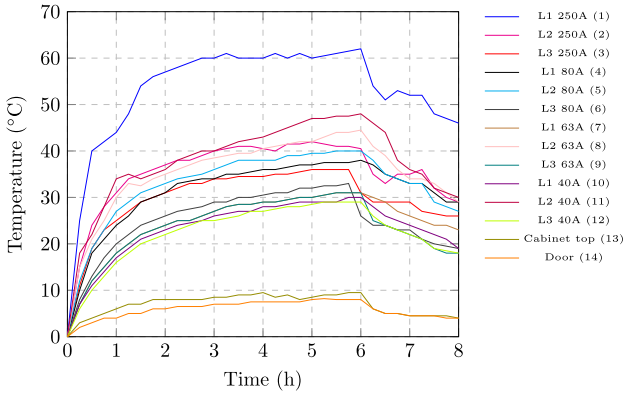

FIGURE 35. Results of circuit heating test.

The results of the circuit heating test are shown in Fig. 35. The test was conducted in accordance with the requirements of the standard [25], [26] and the ambient temperature was 24.4 °C. The maximum temperature rise was achieved at the 250 A supply connection on phase L1 with a value of 61.3 °C. Other locations experienced values between 29.8 °C and 47 °C. Rises in temperature within the housing were 7.9 °C at the door and 9.4 °C on the top surface. The test findings were in compliance with the specifications while taking into consideration that the temperature differences at the measured locations 1 to 14 were not allowed to exceed +70 °C [25]. The test results also meet the requirement that the temperature rise on the housing should not be higher than 30 °C. Fan cooling was activated after the heating test achieved a steady state. The monitored locations recorded temperatures that ranged from 17.0 °C to 29.3 °C, except for the temperature change on phase L1 where it was 45.7 °C.

C. DIELECTRIC TEST OF THE PROTOTYPE

The prototype underwent also a dielectric test. The environmental conditions during the test were ambient temperature of 27 °C and relative humidity of 60%. Dielectric characteristics were examined with a nominal insulation voltage of 1000 V. The test voltage of 2200 V was applied for a duration of 60 s at a frequency of 50 Hz. The specified values were applied between all active parts (phase and neutral conductors) connected to each other and the protective conductor. The test was also conducted between each individual phase and the other phases, connected to accessible conductive parts. During the test, there was no voltage breakdown or overshoot, and the prototype passed the test.

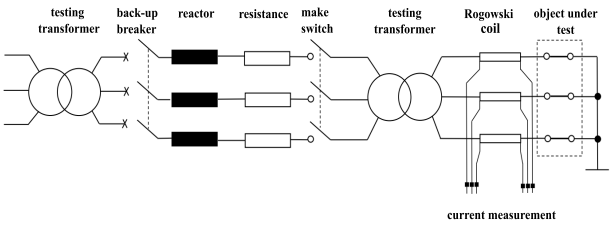

FIGURE 36. Test circuit.

TABLE 10. Results of current test.

Peak value (kA)			Effective current (kA)			Time (s)
L1	L2	L3	L1	L2	L3	
17.4	17	19.2	11.2	11.1	11.1	0.99

D. PEAK CURRENT AND SHORT CIRCUIT CURRENT TEST

The test of the main circuit was carried out (see Fig. 36) with a nominal tolerable peak current value $I_p = 17.0$ kA and a nominal short circuit tolerable current $I_k = 10$ kA, 50 Hz of a nominal duration of 1s. The results are shown in Table 10. After the test, the prototype was visually inspected and no damage was observed. According to the applicable standards [25] and [26], the assembly passed all electrical tests.

E. TENSILE TEST OF THE SCREW CONNECTION

A prototype of the LV electrical cabinet was used also for performing mechanical tests. Tensile tests were run on the bolts and nuts that had been taken out of the switch block and a torque wrench test was used to tighten the bolts on the assembly. For the same reason they had to be subjected to mechanical tests to be verified in accordance with the relevant standard [25], [26]. All tests were performed on threads M4, M6 and M8 on three samples each.

(a) Bolt-nut M4 (b) Bolt-nut M6 (c) Bolt-nut M8

FIGURE 37. Screw connections after tensile test.

TABLE 11. Results of tensile test carried out on screw connections.

Sample bolt	Height (mm)	Cross section (mm^2)	Maximum force (kN)	Tensile strength (MPa)	Surface pressure (MPa)
M4-1	5.88	8.78	2.85	325	68.45
M4-2	5.87	8.78	2.75	313	66.03
M4-3	4.67	8.78	2.77	316	83.80
M6-1	5.88	20.01	5.89	293	93.61
M6-2	5.87	20.1	6.53	325	104.01
M6-3	4.65	20.1	5.81	289	116.75
M8-1	5.85	36.6	10.07	275	119.68
M8-2	4.68	36.6	8.86	242	131.65
M8-3	5.85	36.6	10.47	286	124.47

Testing the resistance of the screw connection to a normalized tensile force and figuring out the tensile force at which the bolt-nut connection would deform was also required. The conditions of the critical area on the bolt and nut under tensile stress were analyzed. To prepare the connection for a typical use of the assembly, the bolt was tightened into place. A 150 kN shredder was used to test the sample, and while the nut was fastened, the bolt was subjected to a tensile force. The

TABLE 12. Results of tensile test carried out on bolts.

Sample bolt	Cross section (mm^2)	Maximum force (kN)	Tensile strength (MPa)
M4-1	8.78	2.83	322
M4-2	8.78	2.85	325
M4-3	8.78	2.82	321
M6-1	20.1	6.89	343
M6-2	20.1	6.35	316
M6-3	20.1	6.23	310
M8-1	36.6	11.68	319
M8-2	36.6	11.82	323
M8-3	36.6	11.68	319

test was carried out until screw connection broke as shown in Fig. 37. The results are shown in Table 11 together with the test results. Also, the highest forces that can be applied to the connection before the bolt breaks or the thread becomes damaged, are provided. The thread surface pressure and the highest measured tensile strength for that particular scenario are also listed.

(a) Bolt M4 (b) Bolt M6 (c) Bolt M8

FIGURE 38. Samples of bolts after tensile test.

(a) Bolt M4 (b) Bolt M6 (c) Bolt M8

FIGURE 39. Samples of bolts in position before bending test.

TABLE 13. Results of bending test carried out on screw connections.

Sample	The force that occurs during deflection (kN)					
	3 mm	4 mm	5 mm	10 mm	15 mm	30 mm
M4-1	0.15	0.17	20.18	0.23	0.25	0.7
M4-2	0.15	0.17	0.19	0.19	0.27	0.69
M4-3	0.14	0.17	0.18	0.21	0.23	0.63
M6-1	0.46	0.57	0.62	0.72	0.79	1.84
M6-2	0.65	0.71	0.73	0.80	0.86	2.25
M6-3	0.56	0.67	0.72	0.80	0.82	2.00
M8-1	1.74	1.85	1.90	2.02	12.14	4.85
M8-2	1.64	31.78	1.84	1.95	2.03	4.62
M8-3	1.72	1.86	1.94	2.10	2.16	4.60

F. TENSILE TESTING OF BOLTS

After the tensile test had been performed on the joint, it was necessary to apply the tensile test on the bolt itself. The bolt was placed in a 150 kN shredder and the pulling force was applied on the head of bolt. The sample was subjected to a controlled tension until fracture. The break occurred on the threads, or more specifically and as expected, where the bolt had a smaller cross section. The results listed in Table 12 show the maximum force and tensile strength of the tested bolts. Fig. 38 shows the state of the test samples after the test.

G. BENDING BOLT TEST (CANTILEVER LOAD)

A potential problem with the connection technology was the load of the joints due to the effect of gravity. Moreover, there was a possibility of the joint to bend due to the weight of the switching devices. As a result, the bolt underwent a bending test in settings similar to those in normal conditions. A bolt was placed horizontally in the breaker and subjected to a bending test as shown in Fig. 39. The test was carried out to a deflection of 30 mm, and the action force was 30 mm from the top of the bolt head. The bolts used in the testing are M4, M6 and M8, and their dimension and shape are given in Table 13. The results of the bending test show the force that occurs during deflection. The outcome of the bending tests run on all samples is that there is no damage. Fig. 40 shows the results of the bending test.

H. TESTING BOLTS BY FASTENING THEM WITH A TORQUE WRENCH (TORSION)

A torque test was performed with a torque wrench on the bolt that was placed in the assembly to verify the security of the connections. Bad connections could result in energy loss and overheating, thus the analysis determined the highest values of the moments at which the bolt would snap. The values were compared with the acceptance criteria defined by calculation. By comparing the values of the criteria defined by the manufacturer and the test results, it was determined that all types of the bolts met the requirements. The reference for the result values was bolt breakage, and all test cases met the criteria as it is shown in Table 14.

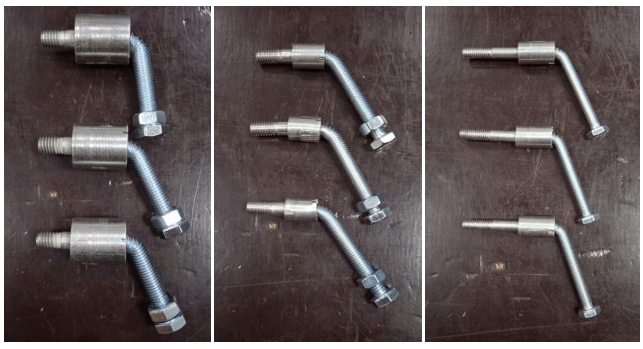

(a) Bolt M4 (b) Bolt M6 (c) Bolt M8

FIGURE 40. Samples of bolts after bending test.

VII. ECONOMIC ASPECTS OF TECHNOLOGY

In terms of initial investment costs, laminated conductors may have a higher upfront cost compared to traditional wire and ducts connections. This is due to the fact that the technology is still rather new and might need specialized production methods and tools. However, over the long term,

TABLE 14. Results of torsion test.

Specimen bolt	Maximum torque (Nm)	Acceptance criteria
M4-1	4.05	
M4-2	3.18	1.5
M4-3	2.78	
M6-1	8.63	
M6-2	11.29	6.0
M6-3	8.26	
M8-1	28.39	
M8-2	25.94	11.0
M8-3	25.06	

laminated conductors may be more cost-effective due to their higher efficiency, reduced production time and maintenance requirements, and improved safety features. The laminated conductor technology can enhance temperature management, minimize the possibility of wire breakage, and increase resistance to vibration and mechanical stress. These qualities could improve the overall dependability of the electrical cabinet, lowering maintenance costs and downtime.

However, the reliability of laminated conductors also depends on proper installation and maintenance. If installed and maintained incorrectly, laminated conductors may be susceptible to failure, which could lead to higher costs and poor reliability. To maximize the advantages of the technology, it is crucial to make sure that suitable installation and maintenance procedures are followed.

To conclude, while laminated conductors may have a higher upfront cost, their improved reliability and reduced maintenance requirements may result in long-term cost savings.

VIII. CONCLUSION

This paper presents the development of a new technology for connecting components in electrical cabinets. If successful, this method would fundamentally alter the way how electrical cabinets are manufactured and maintained. Initial simulation models allowed for the elimination of less successful scenarios and, on the other hand, for the cost-effective production of less test specimens for experimental testing. The critical heating points of each component and the entire assembly were determined using the CFD approach. The temperatures obtained from the thermal simulation of the assembly and each part show that they are within the acceptable range. After simulations had been run, the assembly was verified by experimental testing of heating caused by current conduction. The results showed that all requirements were met. Electrical tests verified the ability of the prototype to withstand dielectric requirements and tests with peak current and short circuit withstand current. Mechanical simulations served as a starting point in the development of a joint that would meet all strength requirements and at a same time fulfill the function of conductive parts of the cabinet. Furthermore, tensile tests were performed on the bolt and the bolted joint, and bending test was performed on the bolt. These tests verified that these components can withstand all stresses that would occur in the operation of the assembly. Torsion on the bolt in the switch block was also tested by tightening the torque wrench, which is a necessary action in every installation of the assembly. The next stage in the development of the prototype would be to assemble a model which would include active components that would be tested for electromagnetic compatibility, which is also final examination according to the requirements for residential and industrial environments. Finally, further work will focus on fully automating the production of electrical cabinets that would be based on the proposed technology.

ACKNOWLEDGMENT

The authors would like to thank Duplico Ltd., Tin Objekt Ltd., and Mehatronika Ltd. (consulting company) for their insightful comments and support. They would also like to thank Končar Ltd. for their help in carrying out the experimental testing.

REFERENCES

[1] S. Spies, M. Bartelt, and B. Kuhlenkötter, "Wiring of control cabinets using a distributed control within a robot-based production cell," in *Proc. 19th Int. Conf. Adv. Robot. (ICAR)*, 2019, pp. 332–337.

[2] F. Hefner, S. Schmidbauer, and J. Franke, "Pose error correction of a robot end-effector using a 3D visual sensor for control cabinet wiring," *Proc. CIRP*, vol. 93, pp. 1133–1138, Jan. 2020.

[3] L. Sun and S. Qu, "Improvement of installation tooling of urban rail electrical cabinet based on TRIZ cutting method," in *Proc. 6th Int. Conf. Mech. Eng. Autom. Sci. (ICMEAS)*, 2020, pp. 232–236.

[4] European Parliament, "Directive (EU) 2019/904 of the European Parliament and of the council of 5 June 2019 on the reduction of the impact of certain plastic products on the environment," *Off. J. Eur. Union*, vol. 155, p. 19, Jun. 2019.

[5] S. Pllana, S. Memeti, and J. Kolodziej, "Customizing Pareto simulated annealing for multi-objective optimization of control cabinet layout," in *Proc. 22nd Int. Conf. Control Syst. Comput. Sci. (CSCS)*, May 2019, pp. 78–85.

[6] J. Davis, *ASM Specialty Handbook: Copper and Copper Alloys*. Metro Parks, OH, USA: ASM International, 2008, p. 600.

[7] K. Anderson, J. Weritz, and J. G. Kaufman, *ASM Handbook: Aluminum Science and Technology*, vol. 2. Almere, The Netherlands: ASM International, 2018.

[8] K. Anderson, J. G. Kaufman, and J. Weritz, *ASM Handbook: Properties and Selection of Aluminum Alloys*, vol. 2. Almere, The Netherlands: ASM International, 2019.

[9] M. C. Leu, A. Ghazanfari, and K. Kolan, "NX 10 for engineering design," Dept. Mech. Aerosp. Eng., Missouri Univ. Sci. Technol., Rolla, MO, USA, 2016, p. 200.

[10] *Technical Reference, Software Version 16, Mentor Graphics*, FloEFD, Wilsonville, OR, USA, 2016.

[11] I. Hadzhiev, D. Malamov, and I. Yatchev, "Influence of overall dimensions and materials of a switchboard on the thermal field distribution," in *Proc. 18th Int. Symp. Electr. App. Technol. (SIELA)*, May 2014, pp. 1–4.

[12] I. Hadzhiev, D. Malamov, I. Balabozov, and I. Yatchev, "Numerical analysis and experimental study of the thermal field in a power distribution block," in *Proc. 19th Int. Symp. Electromagn. Fields Mechatronics, Electr. Electron. Eng. (ISEF)*, Aug. 2019, pp. 1–2.

[13] S. J. Wong and S. S. M. Rafique, "Thermal modelling in product design using FloEFD^{TM} pro: From concept to reality," in *Proc. World Congr. Eng. (WCE)*, 2010, pp. 1–5.

[14] G. Cortella, M. Manzan, and G. Comini, "CFD simulation of refrigerated display cabinets," *Int. J. Refrigeration*, vol. 24, no. 3, pp. 250–260, May 2001.

[15] G. Palanichamy and P. Ahuja, "Unique method for simulation of bolt preload," *Int. J. Eng. Res. Technol.*, vol. 9, no. 10, pp. 734–737, 2020.

[16] J. Kim, J.-C. Yoon, and B.-S. Kang, "Finite element analysis and modeling of structure with bolted joints," *Appl. Math. Model.*, vol. 31, no. 5, pp. 895–911, May 2007.
[17] X. Zheng and W. Xia, "Numerical simulation of blind hole bolt connection with 3-D finite element approach," in *Proc. 2nd Int. Conf. Inf. Comput. Sci.*, vol. 4, 2009, pp. 164–169.
[18] K. Schiffner and C. D. G. Helling, "Simulation of prestressed screw joints in complex structures," *Comput. Struct.*, vol. 64, nos. 5–6, pp. 995–1003, 1997.
[19] I. Hadzhiev, D. Malamov, I. Balabozov, and I. Yatchev, "Analysis of the influence of some factors on the contact resistance of bolted busbar connections," *IOP Conf. Ser., Mater. Sci. Eng.*, vol. 618, Oct. 2019, Art. no. 012025.
[20] R. Dou, T. Ge, X. Liu, and Z. Wen, "Effects of contact pressure, interface temperature, and surface roughness on thermal contact conductance between stainless steel surfaces under atmosphere condition," *Int. J. Heat Mass Transf.*, vol. 94, pp. 156–163, Mar. 2016.
[21] A. Tariq and M. Asif, "Experimental investigation of thermal contact conductance for nominally flat metallic contact," *Int. J. Heat Mass Transf.*, vol. 52, pp. 291–307, Feb. 2016.
[22] Y. Wei, "CFD modeling of thermal contact resistance between solid contacting surfaces," *Energy Sources A, Recovery, Utilization, Environ. Effects*, vol. 40, no. 24, pp. 3009–3018, 2018.
[23] U. Khayam, N. P. Y. Hadisoeseno, S. Harjo, and A. Risdiyanto, "Reducing contact resistance of high current connectors on electric vehicle by controlling contact pressure and addition of plating material," in *Proc. 4th Int. Conf. Electr. Veh. Technol. (ICEVT)*, 2017, pp. 61–64.
[24] *User's Manual FLIR T8xx Series*, FLIR Syst., Wilsonville, OR, USA, 2019.
[25] *Low-Voltage Switchgear and Controlgear Assemblies—Part 1: General Rules*, Standard IEC 61439-1:2011, IEC, 2011.
[26] *Low-Voltage Switchgear and Controlgear Assemblies—Part 2: Power Switchgear and Controlgear Assemblies*, Standard IEC 61439-2:2011, IEC, 2011.
[27] I. Hadzhiev, "Influence of the cables on the heating of a high power low voltage fuse," in *Proc. Youth Forums Sci., Tech., Innov., Bus.*, 2020, pp. 173–176.
[28] *Circuit Breaker, Compact NSX250F, 36 kA/415 VAC, 4 Poles 3D (Neutral Not Protected), TMD Trip Unit 250 A*, Schneider Electr., Rueil-Malmaison, France, Dec. 2020.
[29] *HP 2061 Phenolic Bakelite Paper Sheets*, Bevi, Charlestown, MA, USA, 2020.
[30] European Parliament, "Directive 2014/30/EU of the European Parliament and of the Council of 26 February 2014 on the harmonization of the laws of the Member States relating to electromagnetic compatibility (recast)," *Official J. Eur. Union*, vol. 57, no. L 96, pp. 79–106, 2014.
[31] *User Manual for MultiCon Device Type: CMC-99 X/X/X-1-X-0XX*, Metrix Electron., Bramley, U.K., 2010.

MARIJA ODAK received the B.Sc. and M.Sc. degrees in electrical engineering from the Faculty of Electrical Engineering and Computing, University of Zagreb, Croatia, in 2018 and 2020, respectively. She is currently a Scientific Researcher with the Department of Electric Machines, Drives and Automation, Faculty of Electrical Engineering and Computing, University of Zagreb. She is also employed on the project "Development of technology for connecting components of control electrical cabinets using laminated conductors" funded by EU.

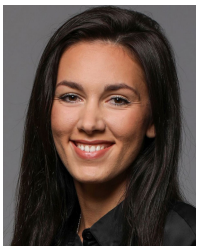

JOSIPA STEGIĆ received the B.Sc. and M.Sc. degrees in electrical engineering from the Faculty of Electrical Engineering and Computing, University of Zagreb, Croatia, in 2018 and 2020, respectively. She is currently a Scientific Researcher with the Department of Electric Machines, Drives and Automation, Faculty of Electrical Engineering and Computing, University of Zagreb. She is also employed on the project "Development of technology for connecting components of control electrical cabinets using laminated conductors" funded by EU.

IGOR ERCEG (Member, IEEE) received the Dipl.Eng. and Ph.D. degrees in electrical engineering from the Faculty of Electrical Engineering and Computing, University of Zagreb, in 2004 and 2010, respectively. He is currently an Associate Professor with the Department of Electric Machines, Drives and Automation, Faculty of Electrical Engineering and Computing, University of Zagreb. His research interests include industrial automation, cybersecurity in process control systems, control of electrical drives, and energy conversion systems.

DAMIR SUMINA received the Dipl.Eng., M.Sc., and Ph.D. degrees in electrical engineering from the Faculty of Electrical Engineering and Computing, University of Zagreb, in 2001, 2005, and 2009, respectively. He is currently a Professor with the Department of Electrical Machines, Drives and Automation, Faculty of Electrical Engineering and Computing, University of Zagreb. His research interests include industrial automation, cybersecurity in process control systems, control of electrical drives, and energy conversion systems.

ELVEDIN TOPČAGIĆ received the B.Sc. and M.Sc. degrees in mechanical engineering from the Faculty of Mechanical Engineering and Naval Architecture, University of Zagreb, in 2015 and 2017, respectively. He is currently an Engineer with Duplico Ltd., on the project "Development of technology for connecting components of control electrical cabinets using laminated conductors" funded by EU.